Smart Structures and Systems, *Vol. 20, No. 4 (2017) 441-450*
DOI: https://doi.org/10.12989/sss.2017.20.4.441

Fiber optic shape sensor system for a morphing wing trailing edge

Monica Ciminello[1], Salvatore Ameduri[1], Antonio Concilio[1],
Ignazio Dimino[1] and Paolo Bettini*[2]

[1]*Adaptive Structures Division, the Italian Aerospace Research Centre, CIRA, Capua (CE), Italia*
[2]*Department of Aerospace Science and Technology, Politecnico di Milano, Italia*

(Received September 15, 2016, Revised August 17, 2017, Accepted August 22, 2017)

Abstract. The objective of this work is to present a conceptual design and the modelling of a distributed sensor system based on fiber optic devices (Fiber Bragg Grating, FBG), aimed at measuring span-wise and chord-wise variations of an adaptive (morphing) trailing edge. The network is made of two different integrated solutions for revealing deformations of the reference morphing structure. Strains are confined to typical values along the span (length) but they are expected to overcome standard ranges along the chord (width), up to almost 10%. In this case, suitable architectures may introduce proper modulations to keep the measured deformation low while preserving the information content. In the current paper, the designed monitoring system combines the use of a span-wise fiber reinforced patch with a chord-wise sliding beam. The two elements make up a closed grid, allowing the reconstruction of the complete deformed shape under the acceptable assumption that the transformation refers to regular geometry variations. Herein, the design logic and some integration issues are reported. Preliminary experimental test results are finally presented.

Keywords: adaptive structures; fiber optic sensors; shape reconstruction; morphing structures control

1. Introduction

With the increasing demand for air travel, improving aircraft efficiency through a more flexible and adaptable aircraft wing design is one of the best ways to reduce aircraft fuel consumption. Modern airplanes exhibit high-level performance, ranging from good carrying capacity up to high cruise speed, high cruise altitude and remarkable climb rates. However, a usual aircraft cannot adapt its configuration with respect to a specific mission or the variable environmental conditions where it is operating. This capability would allow keeping the aerodynamic efficiency around its maximum value instead of suffering variations that can achieve tens of percent. The implementation of morphing wings cam be a key in the attainment of that target. They are supposed to adapt their shape to the specific flight condition, so to minimize the impacts on performance Saristu (2011) and Clean Sky (2016). Such adaptive structures try to mimic nature (Fig. 1) like bird wings that bend and twist to modify their aerodynamic characteristics and match the current needs at the best Barret and Barret (2014). A generic morphing structure requires several integrated subsystems to work together, as for instance:

- A control system, aimed at verifying and stabilizing the congruence of the current shape with the target;
- An actuation system, enabling the attainment of a certain geometry against the action of the external loads;
- A sensor system, able to monitor the actual configuration and feed the control system with reliable inputs.

By providing a suitable feedback, the monitor network gives the control system the possibility to verify the effectiveness of the given commands with respect to the structural elastic response and consequently modify its action (Ko *et al*. 2014, Dimino *et al*. 2014, Pecora *et al*. 2014). As a result, the use of a sensor network becomes even more decisive considering that maintaining the optimal wing shape for each flight condition is fundamental to determine how much better the morphing wing perform than the baseline wing design.

In this paper, the use of fibre optic FBG sensors for the actual shape reconstruction of a morphing wing trailing edge is presented. This solution overcomes most of the common sensor systems limitations, linked for instance to the need of electrical supply, sometimes impracticable packaging, electromagnetic interference with the on-board instrumentation and so on (Jones *et al.* 1996). While keeping a few of the disadvantages of classical systems like cable routing (yet reduced), the use of optical gauges may lead to a dramatic reduction of the wires mass, volume, weight and layout complexity thanks to its multiplexing capability.

Similar applications may be found in the literature for flexible variable camber wing using attached fiber Bragg gratings (Peng *et al.* 2014). An ATED allows attaining quasi-continuous deformation of the aft segment of the wing and targets aircraft aerodynamic performance improvements (Ko *et al*. 2014, Dimino *et al*. 2014).

However, due to the large deformations the resulting

*Corresponding author, Assistant Professor
E-mail: paolo.bettini@polimi.it

ISSN: 1738-1584 (Print), 1738-1991 (Online)

Fig. 1 Biologically inspiration for adaptive aircraft wing

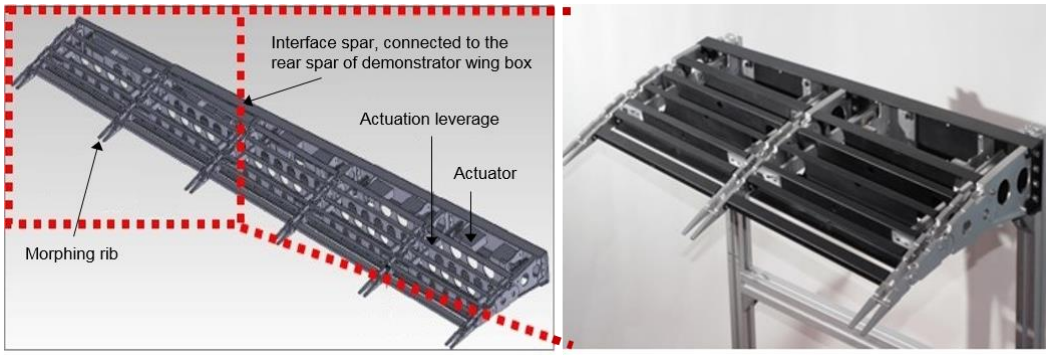

Fig. 2 Digital mock up and dummy adaptive trailing edge device

strain fields may overcome the typical ranges approaching magnitudes up to 10%.

The 2D sensor network herein presented aims at estimating the current shape of a morphing wing Adaptive Trailing Edge Device (ATED); such a device (Dimino *et al.* 2014) allows attaining quasi-continuous deformations of the aft segment of the wing and targets aerodynamic performance improvements in cruise (Ko *et al*. 2014). The network is made of two different components, deployed span-wise and chord-wise. While the former usually experiences deformation values within standard ranges (103-104 με, i.e., 0.01 to 0.1%), the latter can easily record very high levels (104-105 με, i.e., 1 to 10%). In this case, a direct strain measurement would require the use of special and expensive, yet commercial, devices (see for instance Ciminello *et al.* 2013). An adapter is herein proposed in the form of a cantilever beam, designed to cope with the ATED camber line Dimino *et al.* (2013). Then, the paper introduces an original theoretical model for estimating the achieved shape, moving from the discrete set of info, detected by the FBG net. The results of some preliminary experimental tests, carried out to validate the proposed tool, are finally presented.

2. Sensors network description

The sensors network herein addressed, is aimed at monitoring the strain field inside a 2-bay ATED mock-up (Dimino *et al.* 2015). The main structural elements are three kinematic ribs, driven by load-bearing actuators (finger-like systems, whose components are hinged each other) and a main front spar, simulating the attachment to the main wing body (the so-called wing box). Secondary spars are deployed to keep the reference shape (shape spars). The overall demonstrator in-plane dimensions are approximately 800x430 mm, Fig. 2.

The final version of the ATED includes an external deformable skin to guarantee a smooth surface during deformation (Schorsch *et al*. 2015). It is a compound component, made of silicone (deployed at the hinges location and aimed at absorbing the generated strains) and aluminum span-wise elements (aimed at sustaining the aerodynamic pressure load, Schorsch *et al.* 2015). Its presence is not considered in the study ahead, even though some considerations apply directly to its way of working.

Shape variations of the target structure were monitored by two different fibre optic sensor systems, deployed span and chord-wise. In the reference application, they address the classical wing longitudinal bending and the camber morphing, respectively. While the former deformation mode is usually associated to strains ranging between 0.01 and 0.1%, the latter achieves values around many percent units. Because of the selected architecture, in the investigated case these quantities are concentrated at the hinge positions and attain around 50.000 με (5%).

Two main difficulties then arise for a hypothetic sensor: the high strain levels (not suitable for classical commercial, low-cost devices) and the fact that the perspective silicone-based skin is not suitable for bonding any kind of transducer.

An original device is therefore proposed to measure the camber variation through a non-direct measure of the targeted structural deformation (Fig. 3). It is made of a sliding cantilever beam, hosting an integrated fiber optic (FO) system (made of a single fiber or more), free to slide

through the spars and including further sensor elements for balancing thermal variations. The final layout assumes the installation of an FBG for each node (up to a total of three per rib) plus an additional FBG as temperature compensator, assuming the reasonable hypothesis that temperature is constant along the single rib, during operations.

3. Working principles and experimental measurements

3.1 Working principles

An FBG is a confined and systematic discontinuity, printed onto a segment of an optical fiber, reflecting specific wavelengths. For instance, an FBG may be generated by lithography, forcing a periodic variation into the refractive index of the fiber core. Narrowband reflections may be obtained through the deployment of regular discontinuities so that this device can be used to filter certain frequencies.

FBG operation is based on the Fresnel reflection. A broadband light spectrum is transmitted into the optical fiber; when the grating is encountered, a specific wavelength (realistically, a narrow frequency band, centered at the nominal frequency), is reflected and eventually detected by a spectrometer. If strains are applied to the fiber, the gratings period is shrunk or enlarged and reflected wavelengths are in turn modulated.

Because temperature may contribute to the deformation level, additional FBG are typically used as local compensators.

3.2 Instruments

The core of the sensor system is based on a Micron Optics dynamic swept laser interrogator, (MicronOptics, (2016)), associated to a 4x16 optical switch (Fig. 4). In fact, each interrogator channel allows reading a limited number of FBG. Each sensor refers to a characteristic wavelength and extended over a bandwidth interval corresponding to the expected strain variations, the max number of sensible elements on a single fiber is limited and usually set to 12 or 16.

Fig. 4 reports a sketch of the overall system. Its main features are summarized in Table 1.

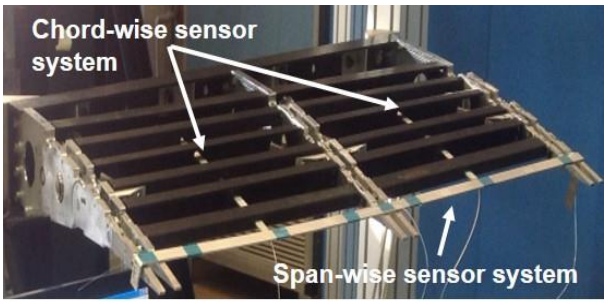

Fig. 3 Adaptive trailing edge sensor network

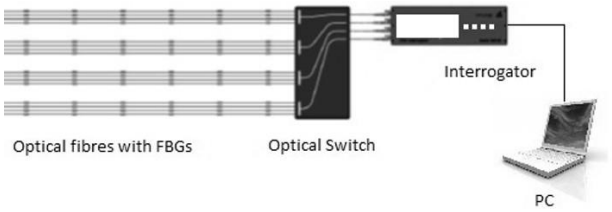

Fig. 4 Sensor system acquisition setup

Table 1 Main characteristics of the sensor system setup

Interrogator	Bandwidth	1 kHz
	Resolution	5 pm
	Power supply	20 W
	Channels	4
Chord-wi sensors Sliding beam	Total number of FBG	6
	Total channels	4
Span-wise sensors Fiber Reinforced patch	Total number of FBG	4
	Total channels	1

3.3 The sliding beam

As previously mentioned, direct measurements of the morphing skin deformation are hard to achieve because of the expected large strain levels and the actual difficulty of bonding whatever on the silicone surface. A modulation transducer is then introduced to overcome this problem. The "sliding beam" is a simple device, made of a thin cantilevered beam that moves within suited spar holes. Friction is held to a minimum value by Teflon covers. One of its extremity is clamped at the rear spar (wing box connection) while the beam length pass through shaped holes manufactured into the other spars while its tip is forced by the trailing edge movement, being this one, the only point where the ATED and the proposed transducer interact. Such a system may be then simulated as a classical clamped beam, forced at its end, Fig. 5.

Its behavior is then described by the well known Eqs. (1)-(3), (Timoshenko and Goodier 1970). The beam thickness can be defined in order to shape the output strain. For the considered architecture, for instance, a 1.5 mm thickness leads to a 22 με deformation for a 0.5 deg deflection; this angular value represents the min observability requirement for the reference ATED, (Bosboom *et al*. 2016, Evenblij *et al.* 2016, Ciminello *et al*. 2015).

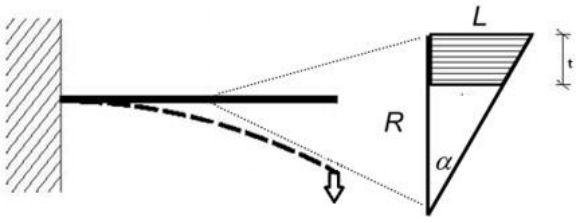

Fig. 5 Simplified model of the strain diagram after a pure bending deformation (upper triangle)

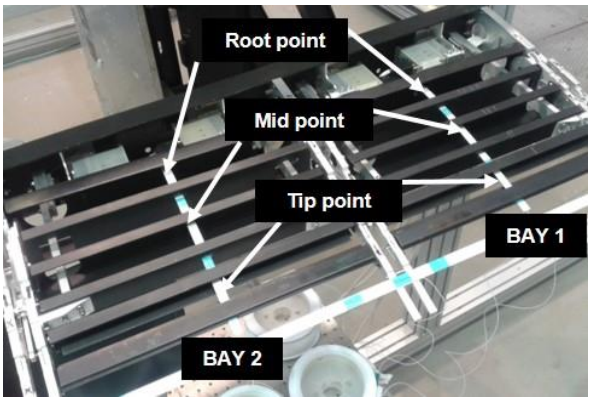

Fig. 6 Sliding beam installation inside the ATED

The selected configuration referred to a single beam to monitor each bay (region between two ribs). On any beam, three FBG sensors are bonded, placed at the corresponding hinges locations. When the ATED morphs, the beam bends and three strain values are detected as a measure of the occurred deflection.

$$\varepsilon(x) = \frac{L_{ext} - L}{L} = \frac{\Delta R}{R} \tag{1}$$

$$\Delta R = \frac{t}{2}; \quad L = R\alpha \tag{2}$$

$$\varepsilon = \frac{t}{2L}\alpha \tag{3}$$

In Fig. 6 a detail of the actual sliding beam installation is shown.

In the application, the baseline configuration is defined as the "non actuated" condition and determines the base signal (occurred strain is set to zero, in turn corresponding to 0 deg angular deflection). When the system morphs up or down, the sliding beams are forced to go upward or downward, respectively and the FBG sensors (installed at the upper surface) record negative (compression) or positive (elongation) strains.

In Fig. 7, time signals are reported for the triplet of sensors, deployed on both the "sliding beams". As shown, the devices follow the actual deformation of the structure, qualitatively well. There are small deviations between namely coincident sensors of the two beams (i.e., placed at the same chord station); they can be related to different reasons, as for instance a non-perfect alignment of the sensors themselves, the non-perfect equivalence of the two bays (the trailing edge was tapered) and so on.

3.4 The sliding beam – governing strain equations

Assuming the deformation function is regular enough, because three data are available (strain at the three sensors), it can be approximated by a second order polynomial, Eq. (4). The unknown coefficients a, b and c may be determined as a function of (ε_1, ε_2, ε_3) by solving the Eq. (5), x_i (i = 1, 2, 3) being the mean stations where the sensors have been installed.

$$\varepsilon_{cw}(x) = ax^2 + bx + c \tag{4}$$

$$\begin{vmatrix} x_1^2 & x_1 & 1 \\ x_2^2 & x_2 & 1 \\ x_3^2 & x_3 & 1 \end{vmatrix} \begin{vmatrix} a \\ b \\ c \end{vmatrix} = \begin{vmatrix} \varepsilon_1 \\ \varepsilon_2 \\ \varepsilon_3 \end{vmatrix} \tag{5}$$

By integrating twice the classical relation between the second derivative of the transversal displacement w_{cv} and the maximum bending strain (measured at the external surface, the largest distance from the neutral axis), Eq. (6),

$$\frac{d^2 w_{cw}}{dx^2} = \frac{2}{t}\varepsilon(x) \tag{6}$$

By imposing the standard boundary conditions for a cantilever beam (zero displacement and zero rotation at the constraint), it follows (longitudinal axis origin at the clamp, x = 0)

$$\begin{aligned} &\frac{dw_{cw}}{dx} = \frac{2}{t}\left[a\frac{x^3}{3} + b\frac{x^2}{3} + cx\right] + K1 \\ &\Rightarrow \left.\frac{dw_{cw}}{dx}\right|_0 = 0; K1 = 0 \end{aligned} \tag{7}$$

$$\begin{aligned} &w_{cw}(x) = \frac{2}{t}\left[a\frac{x^4}{12} + b\frac{x^3}{6} + c\frac{x^2}{2}\right] + K2 \\ &\Rightarrow w_{cw}(0) = 0; K2 = 0 \end{aligned} \tag{8}$$

$$\begin{aligned} &\Rightarrow w_{cw}(x) = \frac{2}{t}\left[a(\varepsilon_1;\varepsilon_2;\varepsilon_3)\frac{x^4}{12}\right] + \\ &+\frac{2}{t}\left[b(\varepsilon_1;\varepsilon_2;\varepsilon_3)\frac{x^3}{6} + c(\varepsilon_1;\varepsilon_2;\varepsilon_3)\frac{x^2}{2}\right] \end{aligned} \tag{9}$$

3.5 Fiber reinforced patches

A dedicated technology was implemented to deploy the fibre along the span, based on the use of special tapes. Taking advantage of their long experience, Politecnico di Milano released this system. In fact, external bonding can appear the simplest method for integrating FO on a generic structure but this procedure hides some difficulties, linked

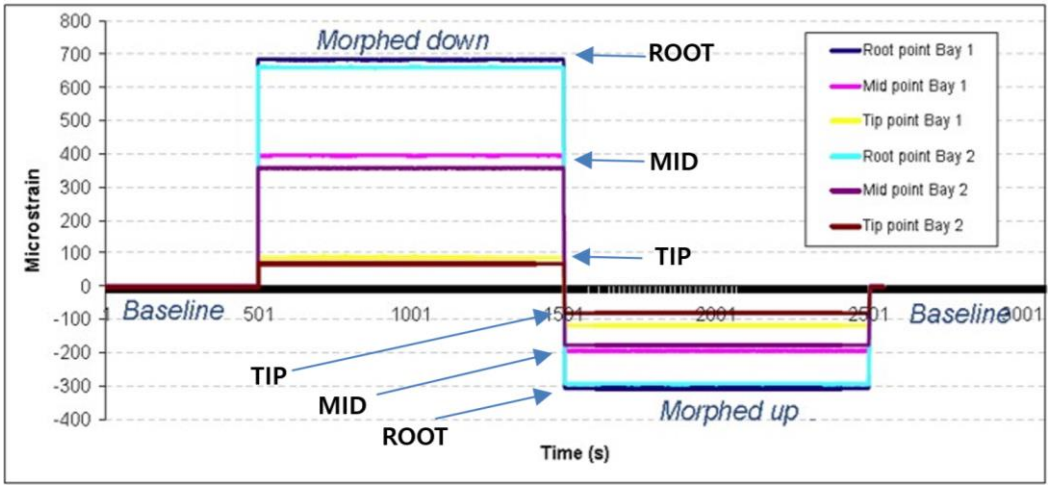

Fig. 7 Acquisition strain from the sliding beam sensors

to the fragility of the fiber and the extremely limited adhesive interface. Thus, sensors installation becomes burdensome and often inadequate. In order to overcome these problems a special patch may be employed, consisting of a thin flexible GFRP laminate (made of glass fibers and epoxy resin) embedding the target FO, Fig. 8.

A dedicated vacuum bag-assisted curing cycle minimizes resin loss and voids percentage around the sensor. The product that is used in this application is named Quick-Pack (QP) and was originally developed by Bettini, Sala and other scientists (Sala *et al.* 2015). Its flexibility is guaranteed by external fabric plies and allows a perfect adhesion also on curved surfaces, while unidirectional (UD) reinforcement fibers at a specific layer preserves FO integrity and operation. The use of polyimide-coated optical fibers, having a glass transition close to 200℃, and guarantees high temperatures process. Among available coating materials, experimental studies demonstrated that epoxy resin exhibits a superior adhesion on polyimide than on other coating materials (Bettini *et al*. 2015, Cassi 2013, Bettini *et al.* 2011), allowing a higher strain transfer capability. The herein used QP presented a lamination sequence made of SAATI SEAL EE48 ET445 prepreg: 48 gsm, 0.05 mm thickness. The curing cycle was set to 30 min at 125℃ and 500 mbar.

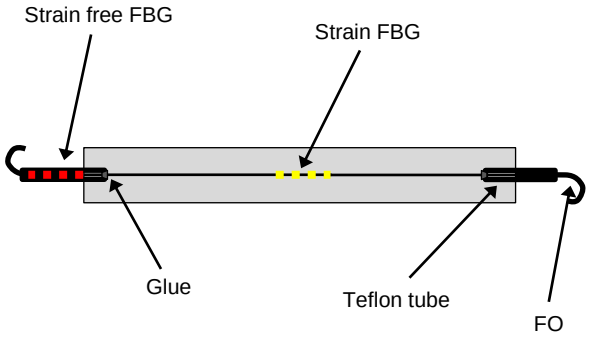

Fig. 8 Sketch of the fiber reinforced patch with strain sensor (yellow) and temperature sensor (red)

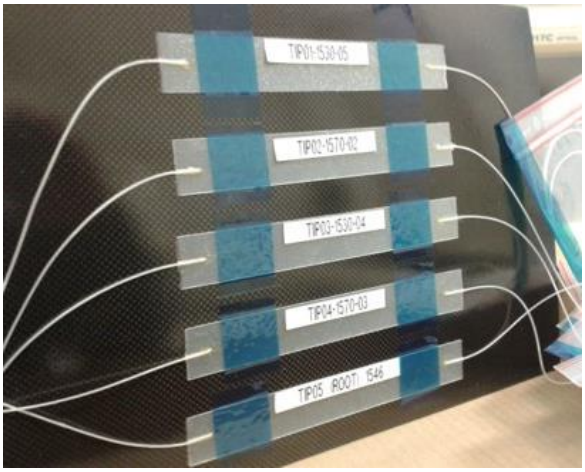

(a)

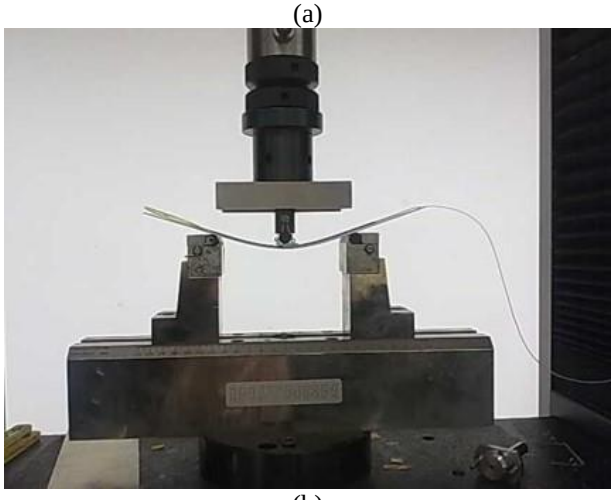

(b)

Fig. 9 Samples of sensor patches (a); 3p bending tests (b)

The external bonding of these special tapes provide many advantages when compared to other available methods such as the direct embedment of FO inside the composite laminates (Bosboom *et al*. 2016):

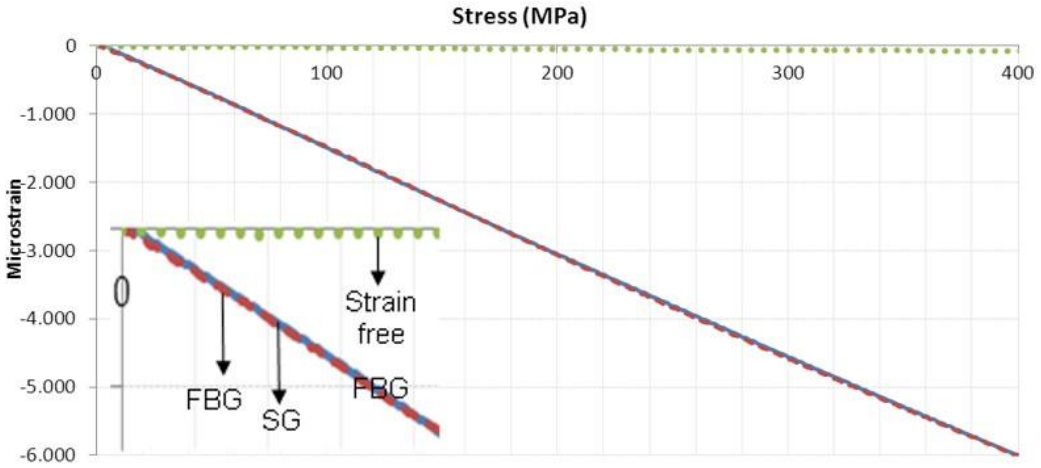

Fig. 10 Experimental gauge factor of the used QP: FBG strain sensor (red dotted line), strain gauge sensor (blue straight line), FBG temperature sensor (green dotted line)

• Lightweight strong protection ensuring ease of handling and integration robustness;
• Capability for large scalable monitoring systems (FO networks) of complex architectures;
• Some repair capabilities (secondary bonding of another tape);
• Surface attachment eliminates issue with ingress and egress of the signal.

The used QPs have an embedded fiber optic inside the laminates, 125 μm diameter and polyimide-coated. Each FO carried two FBG, one located at the middle of the tape and was devoted to strain measures and the other located at the fiber ingress to the pack, deployed into a loose Teflon tube, and devoted to temperature compensation (a correction factor due to the thermal distortion, to be subtracted from the structural measures). In fact, because this last element was not interacting with the structure, a namely strain free condition could be assumed.

In detail, the wavelength shift for FBG sensors obeys the following linear law (Eq. (10))

$$\frac{\Delta\lambda}{\lambda_0} = K_T \Delta T + K_\varepsilon \varepsilon \tag{10}$$

where λ_0 is the nominal center wavelength of the sensor in an unperturbed state, $\Delta\lambda$ is the induced shift, ε and ΔT represent the imposed strain and temperature shift, respectively, and K_T and K_ε are constant, linear scale factors that vary slightly from fiber to fiber and from the central wavelength λ_0.

The wavelength shift is then an indirect measure of the occurring strain that should be however purged of the thermal contribution. In order to give evidence of the magnitude of the cited constants, for germanium-doped silica and for a central wavelength of 1550 nm, K_ε is close to 0.8 while K_T is close to 6.5. Generally, the scaling factors are empirical.

Once embedded, the FBG sensitivity suffers the strain transmission path through the adhesive from the structure.

The global gauge factor of the QP has been characterized through a classical 3p bending test, once it was bonded on aluminum plates representative of the trailing edge tip skin.

The coupons were slowly loaded (velocity rate of 1 mm/min) till a threshold deformation of 6.000 με, twice higher than the expected operative value. As a reference, a standard strain gauge was installed close to the investigated, Fig. 10.

3.6 Fiber reinforced patches – governing equations

In the considered application, it may be assumed that the span-wise beam is pinned to the external ribs tip and clamped to the middle rib tip. At the edges therefore, the strain should be zero (no bending moment) and the displacements should be considered equal to the ones that were already computed for the isolated ribs.

An evenly spaced 4 FBG-array was considered, with measurement points deployed at 1/8, 3/8, 5/8 and 7/8 of the beam span L_s. The strain law was approximated by a 5th order polynomial, coherent with the number of available measurement points and the applicable boundary conditions (y being the span coordinate)

$$\varepsilon_{sw}(y) = ay^5 + by^4 + cy^3 + dy^2 + ey + f \tag{11}$$

A perfect in-plane bending behavior for the referred beam is assumed.

By recalling the Eq. (6) that relates the 2nd derivative of the vertical displacement and the strain distribution, and integrating twice, the displacement can be expressed as

$$w_{sw}(y) = \frac{2}{t}\left(\frac{a}{42}y^7 + \frac{b}{30}y^6 + \frac{c}{20}y^5 + \frac{d}{12}y^4\right) + \\ + \frac{2}{t}\left(\frac{e}{6}y^3 + \frac{f}{2}y^2\right) + K1y + K2 \tag{12}$$

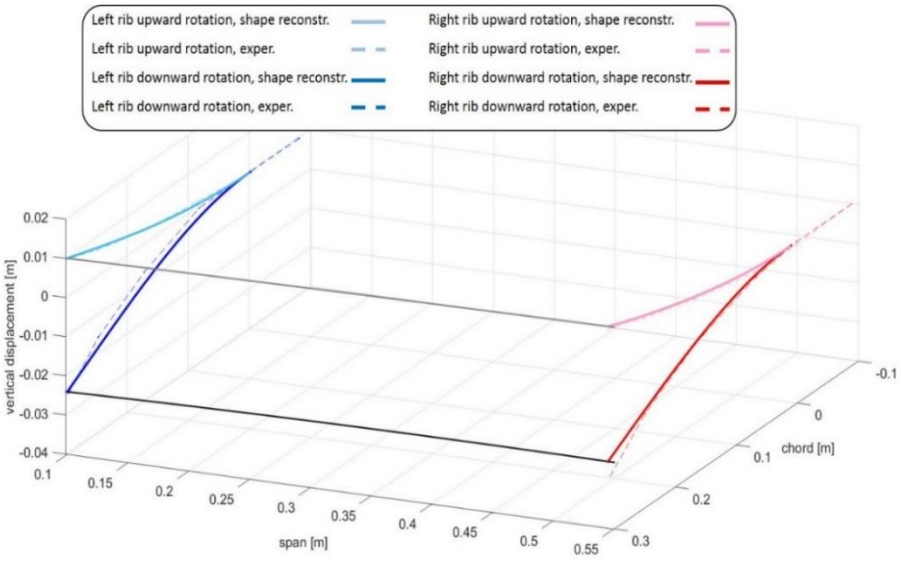

Fig. 11 Sensor system output. Numerical and experimental results are indicated by solid and dot lines, in the order. The black lines describe the deformation recorded by the span-wise sensors

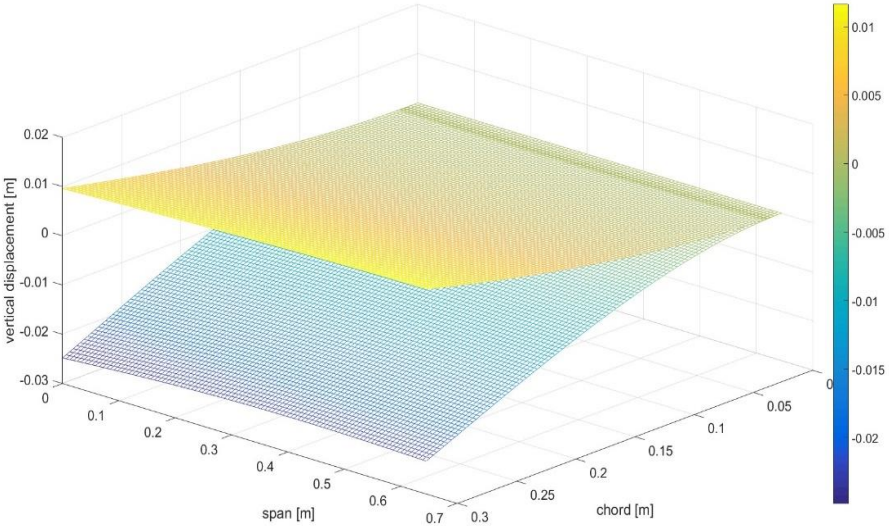

Fig. 12 Parametric surfaces for morphed down and up configurations

By considering the above mentioned boundary conditions

$$w_{sw}(0)=\hat{w}_{sw0}$$
$$w_{sw}(L_s)=\hat{w}_{swLs} \qquad (13)$$
$$\varepsilon_{sw}(0)=\varepsilon_{sw}(L_s)=0$$

the experimental strain values, it is possible to write the linear system Eq. (14), whose solution gives the unknowns *a-f*, K1 and K2.

4. Shape reconstruction

$$\begin{bmatrix} 0 & 0 & 0 & 0 & 0 & 1 & 0 & 0 \\ 1/32768 L_s^5 & 1/4096 L_s^4 & 1/512 L_s^3 & 1/64 L_s^2 & 1/8 L_s & 1 & 0 & 0 \\ 243/32768 L_s^5 & 8/4096 L_s^4 & 27/512 L_s^3 & 9/64 L_s^2 & 3/8 L_s & 1 & 0 & 0 \\ 3125/32768 L_s^5 & 625/4096 L_s^4 & 125/512 L_s^3 & 25/64 L_s^2 & 5/8 L_s & 1 & 0 & 0 \\ 1680/32768 L_s^5 & 249/4096 L_s^4 & 343/512 L_s^3 & 49/64 L_s^2 & 7/8 L_s & 1 & 0 & 0 \\ L_s^5 & L_s^4 & L_s^3 & L_s^2 & L_s & 1 & 0 & 0 \\ 0 & 0 & 0 & 0 & 0 & 0 & 0 & 1 \\ \frac{2}{t}\frac{L_s^7}{42} & \frac{2}{t}\frac{L_s^6}{30} & \frac{2}{t}\frac{L_s^5}{20} & \frac{2}{t}\frac{L_s^4}{12} & \frac{2}{t}\frac{L_s^3}{6} & \frac{2}{t}L_s^2 & L_s & 1 \end{bmatrix} \begin{bmatrix} a \\ b \\ c \\ d \\ e \\ f \\ K1 \\ K2 \end{bmatrix} = \begin{bmatrix} \hat{\varepsilon}_0 = 0 \\ \hat{\varepsilon}_{L_s 1/8} \\ \hat{\varepsilon}_{L_s 3/8} \\ \hat{\varepsilon}_{L_s 5/8} \\ \hat{\varepsilon}_{L_s 7/8} \\ \hat{\varepsilon}_{L_s} = 0 \\ \hat{w}_{sw0} \\ \hat{w}_{swLs} \end{bmatrix} \qquad (14)$$

Table 2 Numerical and experimental deviations

		Chord wise coordinate [m]		
		Root point 0.05	Mid point 0.15	Tip point 0.25
Vertical displacement [m]	Shape reconstructed surface - Right upward	0.0016	0.0039	0.0071
	Exp Right upward	0.0016	0.0038	0.0078
	Δ (Num-Exp)	**0**	**0.0001**	**-0.0007**
	Shape reconstructed surface - Right downward	-0.0018	-0.0083	-0.0163
	Exp Right downward	-0.0012	-0.0081	-0.0195
	Δ (Num-Exp)	**-0.0006**	**-0.0002**	**0.003**
	Shape reconstructed surface - Left upward	0.0014	0.0035	0.0067
	Exp Left upward	0.0009	0.0036	0.0065
	Δ (Num-Exp)	**0.0005**	**-0.0001**	**0.0002**
	Shape reconstructed surface - Left downward	-0.0008	-0.0070	-0.0155
	Exp Left downward	-0.0027	-0.0098	-0.0150
	Δ (Num-Exp)	**0.002**	**0.003**	**-0.0005**

In the experimental campaign, the ATED was forced to assume the established target shape (Dimino *et al*. 2013). The results are reported in Fig. 11, where the vertical displacements of the chord-wise (left and right sliding beams) and the span-wise (longitudinal beam) sensor systems are plotted.

Actual vertical displacements were experimentally measured in morphed up and morphed down configuration, through a Polytec PSV-400 scanning vibrometer.

These measures were compared to the corresponding displacements given by the shape reconstruction process, applied to the measured strain. The error index was defined as the sum of the square errors between the experimental and numerical data, evaluated at each FBG position. The minimization of that error allowed setting the ATED position, accurately.

A maximum deviation lower than 3.0 mm was found in correspondence of the right beam tip (downward movement) and the left beam mid-point (downward movement). In Fig. 12, the deformed surfaces are plotted, having as edges the numerical deformation curves.

5. Conclusions

The task herein described was to reconstruct ATED shape from strain data, retrieved from span and chord-wise sections, using tailored solutions based on FO technologies. Two different kinds of transducers were selected to measure chord-wise and span-wise deformations in order to match geometrical constraints. In particular, a mechanical device (called sliding beam), integrated with an optical fiber sensor system, allows translating shape into strain information along the chord-wise while special reinforced patches (called Quick-Packs) externally bonded to the beam permit direct strain measurements in the other direction. By specific data processing, these strain values are converted into an approximation of the produced shape. The shape reconstruction algorithm was implemented using a commercial Matlab environment. The actual ATED shape was then measured and correlated with the theoretical predictions. The comparison between predicted and reconstructed shape show a good agreement. A maximum deviation lower than 3.0 mm was found out in correspondence of the right downward beam at the tip point and of the left downward mid-point.

The achieved results proved the effectiveness of this technique to identify and quantify the current deflection level of a morphing device. Further improvement can be obtained in terms of measurement precision. For instance, the adoption of distributed optical sensors (Rayleigh backscattering) could guarantee a more detailed description of the strain field. Nevertheless, sensors withstanding larger deformation can enable the measure of the strain directly on the skin, this way achieving detailed information, not only on the displacements of the flap mean line, but also on its external shape. This step plays a fundamental role for the reconstruction of the aerodynamic performance attainable through the morphing device.

Acknowledgments

The work was partially performed within the 7th Framework Programme (FP7, 2007-2013) under the Grant Agreement N.284562 (SARISTU), a funding opportunity gratefully issued by the European Union. In particular, the authors would recall the precious contribution given in that frame by the SARISTU partners Technobis, Inasco and by the CIRA colleague, Pietro Caramuta.

References

Barret, R.M. and Barret, C.M. (2014), "Biomimetic FAA-certifiable, artificial muscle structures for commercial aircraft wings", *Smart Mater. Struct.*, **23**(7), 1-15.

Bettini, P., Di Landro, L., Airoldi, A., Baldi, A. and Sala, G. (2011), "Characterization of the interface between composites and embedded fiber optic sensors or nitinol wires", *Proceedia Eng.*, **10**, 3490-3496.

Bettini, P., Guerreschi, E. and Sala, G. (2015) "Development and experimental validation of a numerical tool for structural health and usage monitoring systems based on chirped grating sensors", *Sensors J.*, **15**(1), 1321-1341.

Bosboom, M.B., Van Wijngaarden, M.J., Evenblij, R., Bettini, P., Loutas, T., Kostopoulos, V., Habas, D., Tur, M., Gorbatov, N., Bergman, A., Ben Simon, U., Kressel, I., Koimtzoglou, C., Ciminello, M., Weisser, A. and Paget, C. (2016), "Ribbon tapes, shape sensors and hardware", *Proceedings of the SARISTU Final Conference, Final Project Conference*, Wölcken, P.C., Papadopoulos, M. (Eds.), Springer, Berlin, Germany.

Cassi, M. (2013), "SHM of composite patch repairs with the use of CFBG sensors", M.D. Dissertation, Politecnico di Milano, Milan, Italy, http://hdl.handle.net/10589/87602

Ciminello, M., Ameduri, S. and Flauto, D. (2013), "Design of FBG based-on sensor device for large displacement deformation", *Proceedings of the IEEE113971IMOC2013*, Rio de Janeiro, August.

Ciminello, M., Dimino, I., Ameduri, S. and Concilio, A. (2015), "Sensor network structural integration for shape reconstruction of Morphing Trailing Edge", *Proceedings of the ICAST2015: 26th International Conference on Adaptive Structures and Technologies*, Kobe, Japan, October.

Clean Sky (2016), http://www.cleansky.eu

Concilio, A., Dimino, I. and Pecora, R. (2016), "An Adaptive Trailing Edge for Large Commercial Aircraft", *Proceedings of the ECCOMAS Congress 2016, 7th European Congress on Computational Methods in Applied Sciences and Engineering*, Crete Island (GK), 5-10 Giugno 2016.

Dimino, I., Ciminello, M., Concilio, A., Gratias, A., Schueller, M. and Pecora, R. (2015), "Control system design for a morphing wing trailing edge", *Proceedings of the 7th ECCOMAS Thematic Conference on Smart Structures and Materials, SMART 2015*, Ponta Delgada (P), 3-6 June 2015.

Dimino, I., Flauto, D., Diodati, G., Concilio, A. and Pecora, R. (2014), "Actuation system design for a morphing wing trailing edge", *Recent Patents Mech. Eng.*, **7**(3), 138-148.

Dimino, I., Flauto, D., Diodati, G., Schüller, M. and Gratias, A. (2013), "Adaptive shape control architecture for morphing wings", *Proceedings of the 6th ECCOMAS Conference on Smart Structures and Materials. SMART2013*, Torino, June.

Evenblij, R., Kong, F., Ciminello, M., Dimino, I., Koimtzoglou, C. and Concilio, A., "Shape sensing for morphing structures using fibre Bragg grating technology", *Proceedings of the SARISTU Final Conference, proceedings of the Final Project Conference*, (Eds., Wölcken, P.C. and Papadopoulos, M.), Springer, Berlin, Germany.

Fausz, J. (2010), "Morphing Flight: Beyond Irreducible Complexity", *Apologetics Press*.

Jones, M.E., Duncan, P.G., Crotts, R., Shinpaugh, K., Grace, J.L., Murphy, K.A. and Claus, R.O. (1996) "Multiplexing optical fiber-based pressure sensors for smart wings", *Proc. SPIE*, Denver, CO, United States, August.

Ko, S., Bae, J. and Rho, J. (2014) "Development of a morphing flap using shape memory alloy actuators: the aerodynamic characteristics of a morphing flap", *Smart Mater. Struct.*, **23**(7), 1-21.

Micron Optics sm130 (2016), http://www.micronoptics.com/products/sensing-solutions/support

Pecora, R., Amoroso, F., Amendola, G. and Concilio, A. (2014), "Validation of a smart structural concept for wing-flap camber morphing", *Smart Struct. Syst.*, **14**(4), 659-679.

Pecora, R., Concilio, A., Dimino, I., Amoroso, F. and Ciminello, M. (2016), "Structural design of an adaptive wing trailing edge for enhanced cruise performance", *Proceedings of the 24th AIAA/AHS Adaptive Structures Conference, AIAA SciTech*, San Diego (CA-USA), 4-7 January 2016, DOI: http://dx.doi.org/10.2514/6.2016-1317.

Peng, L., Yanju, L. and Jinsong L. (2014), "A new deformation monitoring method for a flexible variable camber wing based on fiber Bragg grating sensors", *J. Intel. Mat. Syst. Str.*, **25**(13) 1644-1653.

Sala, G., Di Landro, L., Airoldi, A. and Bettini, P. (2015), "Fibre optics health monitoring for aeronautical applications", *Meccanica*, **50**(10), 2547–2567.

SARISTU (2011), http://www.saristu.eu

Schorsch, O., Lühring, A., Nagel, C., Pecora, R. and Dimino, I. (2015), "Polymer based morphing skin for adaptive wings", *Proceedings of the 7th ECCOMAS Thematic Conference on Smart Structures and Materials, SMART 2015*, Ponte Delgada, Azores, June.

Timoshenko, S.P. and Goodier, J.N. (1970), *Theory of Elasticity*, (3rd Ed.), McGraw-Hill Book Inc., London, UK.

HJ

Nomenclature

FO	*Fiber optic*
FBG	*Fiber Bragg Grating*
ATED	*Adaptive trailing edge*
L	*Beam length*
R	*Curvature radius*
T	*Beam thickness*
α	*Curvature*
ε	*Deformation*
X	*Integration variable in the longitudinal direction*
W	*Vertical displacement*
K1	*Integration constant*
K2	*Integration constant*
cw	*chord wise*
sw	*span wise*
GFRP	*Glass fiber reinforced panel*
QP	*Quick pack*
UD	*Unidirectional*